Resonance-enhanced multiphoton ionization of atomic hydrogen

L. R. Brewer* and F. Buchinger†
Research Laboratory of Electronics and Department of Physics, Massachusetts Institute of Technology, Cambridge, Massachusetts 02139

M. Ligare‡ and D. E. Kelleher
National Institute for Standards and Technology, Gaithersburg, Maryland 20899
(Received 31 March 1988; revised manuscript received 31 October 1988)

We have measured the resonance-enhanced four-photon ionization of atomic hydrogen. The degenerate four-photon process occurs via a three-photon resonance between the 1*s* and the 2*p* levels, with subsequent one-photon ionization near threshold. We have studied the highly asymmetric resonance-enhanced profile, i.e., the photoion yield as a function of laser detuning from three-photon resonance between the 1*s* and 2*p* levels. In particular, we have determined the width, shift, peak, and asymmetry of the profile as a function of laser intensity. The experimental results are compared to theoretical models. These models involve both the properties of the atom in an intense near-resonant radiative field, and a detailed model for the multimode laser field, particularly the field fluctuations due to mode beating. The asymmetric resonance-enhanced photoionization profile is well reproduced by both a random-phase and a chaotic-light model.

I. INTRODUCTION

We report a detailed study of resonance-enhanced multiphoton ionization of atomic hydrogen, using a single high-power pulsed tunable laser. Three photons with wavelength $\lambda = 365$ nm excite the 1*s*-2*p* transition, and a fourth photon from the same laser pulse photoionizes the atom very near its ionization threshold (see Fig. 1). The laser frequency in this experiment was tuned through the three-photon 1*s*-2*p* resonance to observe the ion-yield profile associated with resonance enhancement of the four-photon ionization. Profiles for this photoionization scheme were reported by Tjossem and Cool and by Alden *et al.*[1] The purpose of the present paper is to expand upon an earlier quantitative interpretation of our results[2] and to present further experimental and theoretical results.

According to the nonrelativistic theory of the hydrogen atom, the energy difference between the $n = 1$ and $n = 2$ levels is exactly three-fourths of the energy needed to ionize the atom. In this case the fourth photon in our ionization scheme would lead to excitation exactly at threshold. In actuality, however, relativistic and QED effects shift the energies of the levels. In the absence of external fields the net result is that four photons with exactly one-third the energy of the $1\,^2S_{1/2} \rightarrow 2\,^2P_{3/2}$ transition provide enough energy to ionize the atom, while four photons with exactly one-third the energy of the $1\,^2S_{1/2} \rightarrow 2\,^2P_{1/2}$ transition have an energy which lies just below the ionization threshold. In the intense laser fields of our experiment the bound energy levels will be further altered by the ac Stark shift, and the ionization threshold will be shifted up by the related ponderomotive potential. The largest of these effects is the upward ac Stark shift of the 2*P* levels, and at all the laser intensities used in this experiment this shift is sufficient to increase the energy of the resonant photons to the point that the fourth photon will provide sufficient energy for ionization for either of the intermediate states. Thus photoionization is energetically allowed, even without considering such effects as field ionization by the small electric field that we use to extract the ions.

In our experiments the observables are the width, shift, and shape (i.e., asymmetry) of the resonance-enhanced photoionization profile generated as we tune the laser

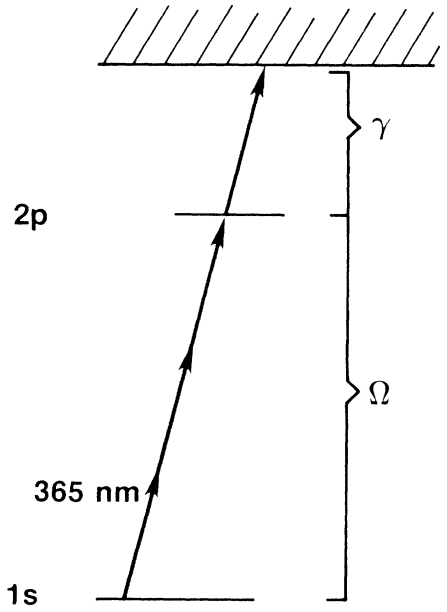

FIG. 1. Excitation scheme for the four-photon ionization of atomic hydrogen. The hydrogen 2*p* level is populated by three photons with $\lambda = 364.6$ nm and a fourth photon of the same wavelength ionizes the atom near threshold. Ω is the three-photon excitation rate of the 2*p* state; γ is the one-photon ionization rate of the 2*p* state.

through the three-photon transition to the $n=2$ level. Also, we measured the dependence of the peak of this profile as a function of the absolute laser intensity.

In our photoionization scheme, the three-photon Rabi rate Ω driving population between the $1s$ and $2p$ states is much slower than the subsequent one-photon ionization rate γ of the $2p$ state. The relatively slow Rabi rate constitutes the "bottleneck" for the photoionization, and virtually any excitation to the $2p$ state will be followed by photoionization. The lifetime, and thus the width, of the $2p$ state in the radiative field is dominated by its one-photon ionization rate.

For a given laser intensity, the net photoionization rate in this case is a function of the three-photon excitation rate times the "shape function" associated with the broadening and shifting of the $2p$ level. Both the width and the shift of the profile vary linearly with laser intensity. These points will be discussed in detail in the next section.

To model the resonance-enhanced multiphoton ionization we require a knowledge of the effect of the radiative field on the atom. This includes the evaluation of the Rabi rate between the ground and excited states, and the width and shift of the resonance-enhanced profile for a given radiative field.[3] We also require a detailed knowledge of the time dependence of the radiative field $E(t)$. For a multimode laser, $E(t)$ can be quite complicated, and vary significantly from one laser shot to the next. A useful model for $E(t)$ and the effect it has on the resonance profile (for the case where the photoionization rate of the intermediate resonance exceeds its excitation rate) has been published by Zoller.[4]

II. THEORETICAL MODEL

Multiphoton ionization can be treated most simply in laser fields of constant amplitude. Holt, Raymer, and Reinhardt[3] have studied the time dependence of resonant multiphoton ionization of atomic hydrogen in constant laser fields and demonstrated that for three-photon resonant, four-photon ionization there exists a time interval during which a time-independent rate of ionization can be defined. For the ionization channel involving the $2p$ state this rate, R, is given by

$$R=|\mu_{12}^{(3)}\varepsilon^3|^2\frac{\gamma}{[3\omega_L-\omega_{12}-(\delta_2-\delta_1)]^2+(\gamma/2)^2}\ , \tag{1}$$

where $\mu_{12}^{(3)}$ is the third-order effective matrix element coupling the $1s$ and $2p$ states, ω_L is the laser frequency, ω_{12} is the unperturbed $1s$-$2p$ transition frequency, γ is the single-photon ionization rate of the $2p$ state, δ_1 (δ_2) is the ac Stark shift of the $1s$ ($2p$) state due to the laser-induced mixing of the $1s$ ($2p$) state with all other atomic levels, and ε_0 is the amplitude of the laser field defined by

$$\varepsilon(t)=\varepsilon_0 e^{i\omega t}+\text{c.c.} \tag{2}$$

The three-photon Rabi rate Ω is given by $\Omega=2\mu_{12}^{(3)}\varepsilon_0^3$. The following values of the parameters used in this investigation were calculated by Reinhardt using the Floquet techniques of Ref. 3: $\Omega=(3.63\times10^2)\varepsilon_0^3$, $\delta_2-\delta_1=(1.27\times10^2)\varepsilon_0^2$, and $\gamma=(1.01\times10^2)\varepsilon_0^2$, where all quantities are in atomic units.

The rate predicted by Eq. (1) is simply the rate at which population is lost from a driven two-level system. The rate constant γ reflects the rate of loss from the excited state due to photoionization. Equation (1) is valid for times $t\gg1/\gamma$ long enough that all transient effects associated with the turning on of the laser have died out, and for times short enough that the ground state is not significantly depopulated, i.e., $Rt\ll1$. This further requires that the field strength be such that $\gamma\gg|\mu_{12}^{(3)}\varepsilon_0^3|$. In this limit, the $1s$-$2p$ transition represents the rate-limiting step or bottleneck of the ionization process. For our experimental conditions, collisional and radiative processes which compete with the depopulation of the $2p$ state by photoionization have rates several orders of magnitude smaller than γ and thus do not appear in Eq. (1). We note that the rate of direct four-photon ionization through virtual states excluding the 2p state is negligible at the field intensities of our experiment so that interference between these processes is insignificant.[5]

The resonance-enhanced ionization line shape predicted by Eq. (1) has a symmetric Lorentzian profile whose center is shifted in frequency from the unperturbed three-photon $1s$-$2p$ resonance by the net ac Stark shift of the $1s$ and $2p$ states. The width of the profile is determined by the single-photon ionization rate of the excited $2p$ state, which determines the lifetime of this state. Although the ionization probability integrated over the detuning frequency increases as the cube of the laser intensity (since the rate-limiting Rabi excitation is a three-photon process), the peak of the predicted ionization rate grows only with the square of the laser intensity. This is because the loss rate from the $2p$ state due to photoionization, and thus the width of the profile, grows linearly with the intensity of the laser. This effect can be seen simply by noting that the peak rate given by Eq. (1) always occurs when $3\omega_L-\omega_{12}-(\delta_2-\delta_1)=0$, which leaves a quartic intensity dependence in the numerator and a quadratic dependence in the denominator.

The constant-amplitude field used in deriving Eq. (1) is not a good approximation to the field of the high-power laser used in this and many other multiphoton ionization experiments. The measurements described in the experimental section of this paper demonstrate that our laser spectrum consists of many longitudinal cavity modes spanning a full width at half maximum (FWHM) bandwidth of $B=0.25\ \text{cm}^{-1}$. This finite bandwidth leads to pronounced intensity fluctuations occurring on a time scale characterized by $1/B\sim0.1$ nsec, and an accurate description of the nonlinear ionization process must account for these fluctuations of the field amplitude. These fluctuations about the mean laser intensity lead to substantial enhancements of the observed widths and shifts over those predicted by Eq. (1), as well as a pronounced asymmetry of the ionization profile. The asymmetry arises from the distribution of instantaneous ac Stark shifts (always to the blue in our case) which result from the variation of intensity within each ionizing laser pulse.

The observed ion yield is also influenced by the spatial

distribution of field intensities at the focus of the laser. Individual atoms experience fields which are dependent on their position, and any model that predicts measured total ionization yield must integrate the yield for atoms at various locations within the laser beam over the spatial profile of the beam.

When calculating the time-dependent rate of resonant multiphoton ionization in finite-bandwidth fields it is easiest to employ a semiclassical description of the ionization process because of the advantages afforded by the use of a classical electromagnetic field when describing laser pulses whose amplitude varies in time. The general density-matrix equations governing resonant multiphoton processes have been discussed in Ref. 6, and are reviewed in the Appendix. Equation (1) no longer gives an accurate prediction for the experimentally observed ionization profile in the case of finite-bandwidth excitation. However, if the one-photon ionization of the excited state occurs rapidly on the time scale of the field fluctuations, i.e., if $\gamma/2\pi \gg B$, then the ionization can be considered to have occurred at a fixed value of the field. In this case Eq. (1), with the values of $\varepsilon(t)$, $\gamma(t)$, and $\delta(t)$ corresponding to the instantaneous value of the field, will give an instantaneous time-dependent rate of ionization. These ideas are developed more completely in the Appendix.

To obtain a prediction of the experimentally observed ion yield as a function of laser frequency, the rate of ionization must be integrated over the temporal and spatial distributions appropriate to the laser pulses used. For atoms that are sufficiently slow so that they do not move out of the focus of the laser in the time of a single laser pulse, the number of ions, N, created in a pulse will be given by

$$N=\int dt \int d\mathbf{r}\, p(\mathbf{r})R(\mathbf{r},t)\ , \tag{3}$$

where $p(\mathbf{r})$ is the density of atoms and $R(\mathbf{r},t)$ is the generalized time- and space-dependent ionization rate which is equivalent to Eq. (1), except that the quantities ε, γ, and δ are now functions of $\mathbf{r}$ and t. We have analytically integrated the spatial variables of Eq. (3) over the radial profile of a Gaussian laser beam and numerically integrated over time using a simple model of the laser field behavior as a function of time.

For a Gaussian laser beam the generalized ionization rate becomes

$$R(\mathbf{r},t)=|\mu_{12}^{(3)}\varepsilon_0^3(t)|^2\frac{\gamma_0(t)e^{-4r^2/w^2}}{[3\omega_L-\omega_{12}-\delta_0(t)e^{-r^2/w^2}]^2+\frac{1}{4}[\gamma_0(t)e^{-r^2/w^2}]^2}\ , \tag{4}$$

where $\varepsilon_0(t)$, $\gamma_0(t)$, and $\delta_0(t)$ are, respectively, the values for the field strength, $2p$-state ionization rate, and net Stark shift at the spatial center of the beam at the beam waist. For a Gaussian beam with a waist w, small compared to the scale of variations in $p(\mathbf{r})$, we have performed the integration of Eq. (3) over the radial coordinate to simplify the expression for the total ion yield as a function of the laser detuning, $\Delta=3\omega_L-\omega_{12}$:

$$I(\Delta)=\frac{\pi\omega^2 g G_4\delta_0^2}{4(1+g^2)^2}\left\{1+g^2+\frac{4\Delta}{\delta_0}+\frac{\Delta^2(3-g^2)}{\delta_0^2(1+g^2)}\ln\left[1-2\frac{\delta_0}{\Delta}+\frac{\delta_0^2(1+g^2)}{\Delta^2}\right]\right.$$
$$\left.+\frac{2}{g}\frac{\Delta^2(1-3g^2)}{\delta_0^2(1+g^2)}\left[\tan^{-1}\left[\frac{\delta_0(1+g^2)}{g\Delta}-g^{-1}\right]+\tan^{-1}(g^{-1})\right]\right\}\quad(\Delta\neq 0)\ . \tag{5}$$

In performing this integration we have taken advantage of the fact that the ionization rate of the $2p$ state, γ_0, and the net ac Stark shift, δ_0, are both proportional to the laser intensity, and thus the numerical factor $g=\gamma_0/2\delta_0$ in Eq. (5) is independent of the field intensity, as is G, defined as $\Omega^2\delta^{-3}$.

To complete our treatment we have made a model of the temporal behavior of our laser pulses which is based on the measured properties of our laser as reported in the experimental section of this paper. For a laser cavity with more than one longitudinal mode, mode beating gives rise to pronounced intensity fluctuations within each laser pulse. The beat frequencies for n modes range up to $nc/2L \sim B$ where L is the optical length of the laser cavity. In our model we write the field as a sum over independent modes with each mode having a randomly determined phase with respect to the other modes. The complex field amplitude is then given by summing over the j modes:

$$\varepsilon(r,t)=e^{-t^2/2\tau^2}e^{-r^2/2w^2}\sum_j a_j e^{-i(\Delta\omega_j t+\phi_j)}\ . \tag{6}$$

Each mode has an amplitude a_j, phase ϕ_j, and frequency detuning $\Delta\omega_j$ from the center laser frequency ω_L. The relative mode amplitudes are chosen to match the measured Gaussian spectrum about the central laser frequency and they are normalized to give the correct total energy per laser pulse. The factor $\exp(-t^2/2\tau^2)$ reflects the overall time envelope of the pulses, and the factor $\exp(-r^2/2w^2)$ reflects the previously discussed spatial profile of the laser beam.

Typical temporal behavior of model pulses resulting from Eq. (6) are shown in Fig. 2(a). The pulses for 1, 3, 7, and 15 modes all have the same energy, with the mode

separation given by 1 GHz. It is clear that the mode beating characteristic of the conditions in our laser leads to intensity spikes well above the mean intensity. It is the effective concentration of the photon flux into these high-intensity spikes which enhances the observed shifts and widths in multiphoton ionization experiments. The exact simulated pattern generated by Eq. (6) varies from "shot to shot" due to the randomly generated phases for each shot [see Fig. 2(b)]. We note that the time behavior displayed in Fig. 2 is similar to that observed for other multimode pulsed lasers.[7] This is also the case for our experimental time behavior presented later in this paper.

The ion yield as a function of detuning has been calculated by performing the integration indicated in Eq. (3) over 60 simulated laser pulses with 15 modes and random intermode phases, and the result is displayed in Fig. 3(d). The pulses used to generate the profiles in Fig. 3 had an energy of 5.8 mJ, $\tau = 5.4$ nsec, and $w = 32$ μm, corresponding to our experimental conditions. In order to demonstrate the large effects of both the spatial and temporal inhomogeneities which have been combined to give the integrated ionization profile of Fig. 3(d), we have plotted the theoretical profiles from other idealized pulses in Figs. 3(a)–3(c). All pulses used in generating Fig. 3 have equivalent temporal and spatial widths, and were normalized to have energies of 5.8 mJ. In order to facilitate the comparison of the shapes of the profiles, and because we did not experimentally measure absolute ionization cross sections, we have adjusted the heights of all the profiles to be equal. We note, however, that the peak of profile 3(d) is predicted by our analysis to be a factor of 4 greater than the peak of 3(a).

The Lorentzian profile for uniform intensities predicted by Eq. (1) is displayed in Fig. 3(a), while the result of averaging Eq. (1) over a Gaussian spatial intensity distribution is given in Fig. 3(b). Figure 3(c), which is the result of averaging over Gaussian spatial and temporal distributions, corresponds to the result from a Fourier-transform-limited single-longitudinal-mode laser. Even this "best-case" laser results in significant differences

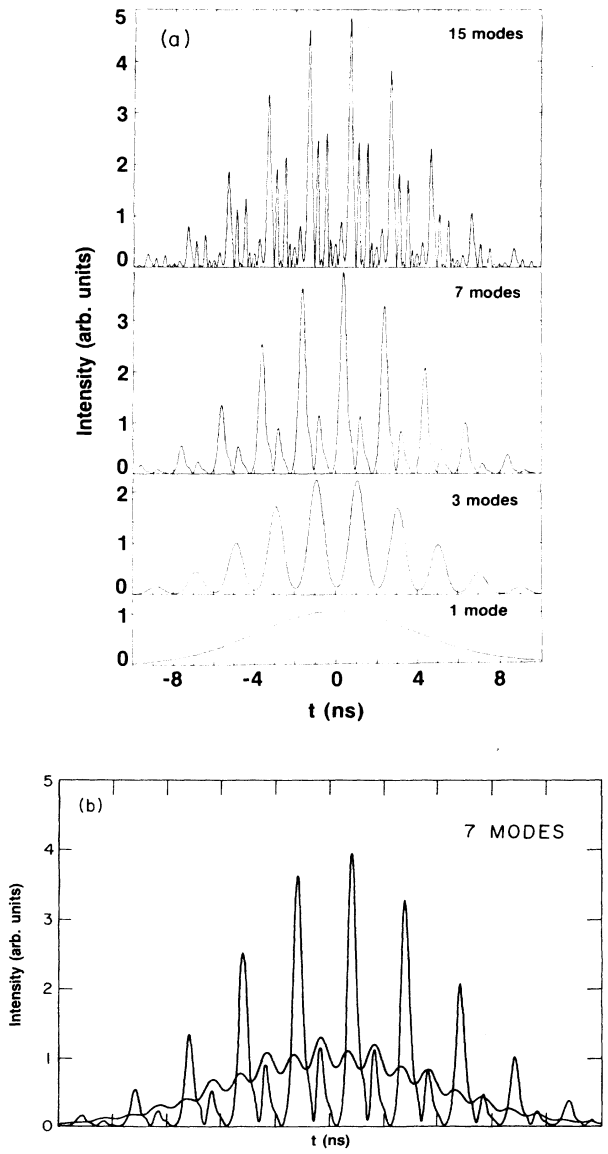

FIG. 2. (a) Typical time dependence of a laser pulse with 1, 3, 7, and 15 longitudinal modes. (b) Time dependence of two laser pulses with seven modes, but different sets of random phases between the modes. In generating the computed ionization profiles such as those in Fig. 3, we used 60 different sets of random phases to generate each point along the profile.

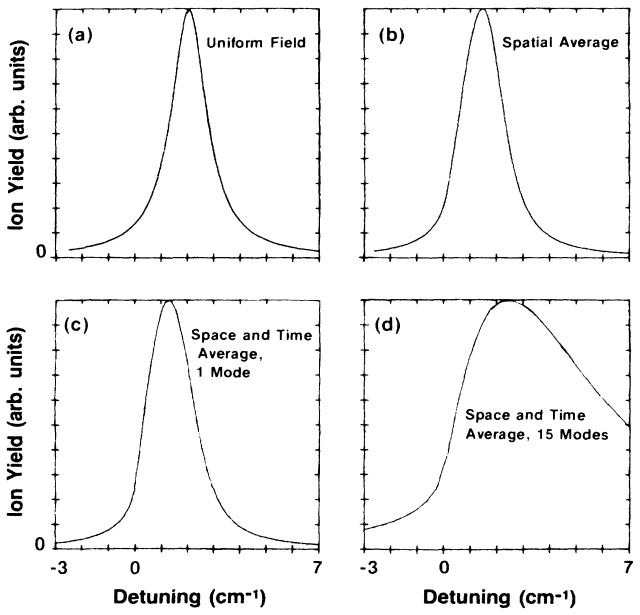

FIG. 3. Resonance-enhanced ion-yield profiles to illustrate the relative importance of different contributions. (a) Yield from uniform laser in space and time, (b) yield averaged over Gaussian spatial distribution of the focused beam, (c) yield averaged over Gaussian spatial and temporal envelopes, but no mode beating, and (d) yield averaged over spatial and temporal inhomogeneities of a multimode laser.

from the profile predicted for uniform fields. Figure 3(d) includes the effects due to the temporal fluctuations of a multimode laser, and these give by far the largest modifications to the profile.

Unlike the pronounced effect of the field fluctuations on the shift, width, and shape of the ionization profile, the intensity dependence of the peak of the ion yield is not affected by the fluctuations as long as the instantaneous ionization rate can be written in the form of Eq. (1).[8] This invariance holds in a statistical sense for any ensemble of pulses which is large enough to completely sample the intensity distribution of the laser field, i.e., the combined pulse durations must be much greater than B^{-1}. Thus our model predicts that the peak of the resonance profile should grow with the square of the laser intensity. Deviations from this dependence will arise whenever an instantaneous rate in the form of Eq. (1) is not a valid approximation. This simple formula breaks down whenever the bandwidth of the laser is large compared to the single-photon ionization rate of the excited state, i.e., $B > \gamma/2\pi$ (see the Appendix). In this limit the field fluctuates significantly during the characteristic ionization time of the $2p$ state, and the ionization cannot be considered to have occurred at a fixed value of the field. We note that Zoller[4] has considered the effects of such rapid fluctuations for the case of a field which can be characterized by Gaussian statistics. We have also neglected the small Doppler width of the $1s$-$2p$ transition, which would modify slightly the form of Eq. (1).

III. EXPERIMENT

Tunable 365-nm (uv) light was generated using the technique of Zacharias *et al.*[9,10] The laser setup is shown in Fig. 4. The oscillator, a Littman-type near-grazing-incidence ($\sim 5°$) dye laser[11] with prism beam expander, was tuned to a wavelength of approximately 555 nm. The laser dye was Rhodamine-6G in triflouroethanel solvent. Light from the oscillator was amplified by two longitudinally pumped amplifiers and then frequency sum mixed in a potassium dihydrogen phosphate (KDP) crystal (type II) with the 1064-nm Nd:YAG (yttrium aluminum garnet) fundamental (ir) to produce 365-nm uv radiation.

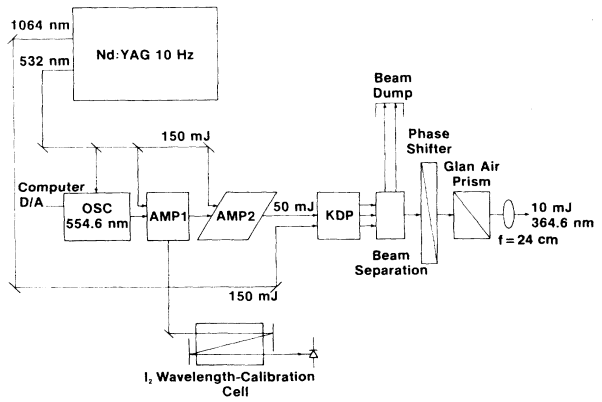

FIG. 4. Schematic view of the laser setup used for the four-photon resonance ionization of atomic hydrogen.

The KDP crystal was phase matched by angle tuning. During a 12-cm^{-1} scan of the dye laser, the uv laser power was kept constant to within 10% by monitoring the power at several frequencies and phase matching the crystal manually. During a scan of 12 cm^{-1} (0.15 nm at 365 nm) only slight adjustments were needed. Typically 55 mJ of dye-laser light was converted to 10 mJ of ultraviolet laser light by sum mixing with 150 mJ of the Nd:YAG fundamental. The ir, uv, and dye-laser beams were separated using a trio of Pellin-Broca prisms.

Because measurements of the resonance-ionization profile were made as a function of the laser-pulse energy it was important to be able to vary this quantity without changing the spatial properties of the laser beam. For this purpose we used a polarization rotator (Soleil-Babinet compensator) and analyzer (Glan-Air polarizer). The uv beam was focused into the interaction region by a diffraction-limited 240-mm-focal-length lens.

The uv laser-pulse energy was measured with a volume-absorbing disk calorimeter. The overall instrumental accuracy of this combination was 5%. The pulse-to-pulse fluctuations of the uv light were measured with a photodiode. They were found to be $\pm 22\%$ (one standard deviation) of the mean laser intensity.

The wavelength of the uv laser light was determined by measuring the wavelength of the tunable dye laser to an accuracy of 0.05 cm^{-1} using an iodine absorption cell. The second harmonic of the Nd:YAG fundamental wavelength was measured to be 532.09 ± 0.01 nm (in air) giving the fundamental wavelength of 1064.18 ± 0.02 nm (in air). The frequency of the uv light was determined to an accuracy of 0.2 cm^{-1}.

An air-spaced étalon with a free spectral range of 1.1 cm^{-1} and a finesse of between 25 and 30 was used to determine the linewidth of the uv light. The intensity of light transmitted by the étalon was measured by a photodiode as the laser frequency was scanned. The linewidth of the uv light (FWHM) was 0.25 ± 0.05 cm^{-1}. To check the frequency jitter of the uv laser source the linewidth was also measured by imaging the étalon fringes onto a linear diode array, displaying the results on an oscilloscope and photographically recording the single-laser-shot fringe pattern. This measurement was in agreement with the first.

The number of longitudinal cavity modes can be approximately calculated. The full width half maximum of the tunable dye laser output was $B' = 0.1$ cm^{-1}. The full width at one-tenth maximum was 0.18 cm^{-1}. The tunable-dye-laser cavity length L was 35 cm. The spacing between longitudinal modes was $1/2L = 0.014$ cm^{-1} and the number of modes was 13.

The diameter of the uv laser beam at the focus was measured with a photodiode array. The laser light was attenuated to several different intensities and the resultant profiles were examined to make sure the diode array was not saturated. Individual laser shots were fit to a Gaussian in laser intensity, $I \sim e^{-r^2/w^2}$. A typical spatial profile is shown in Fig. 5 along with a least-squares fit. For diode array axes both parallel and perpendicular to

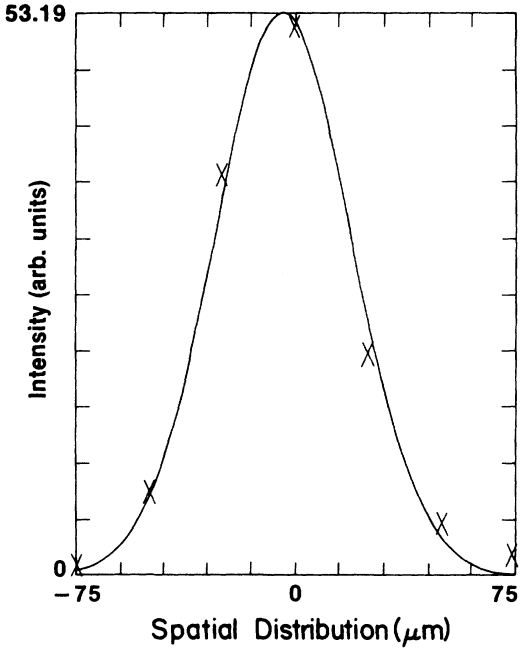

FIG. 5. Spatial distribution of the laser-beam intensity (crosses). The profile was measured at the focus of the $f=240$ mm lens used for focusing the $\lambda=364.6$ nm light into the interaction region. The solid line represents a least-squares fit to the data using a Gaussian distribution.

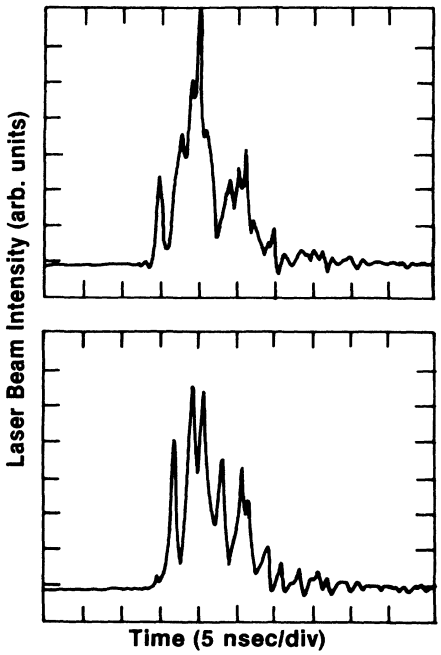

FIG. 6. Temporal profile of the laser-light pulse for two arbitrary pulses. The spikes on the signals and their different temporal structure indicate the presence of many laser-cavity modes with random-phase relations (see text).

the laser polarization $w=32\pm3$ μm. This corresponds to a full width half maximum of 53 ± 5 μm.

The temporal profile of the ultraviolet laser pulse was measured using a fast photodiode-oscilloscope system with a combined rise time of 600 psec. Figure 6 shows two temporal pulse profiles. These profiles can be compared to the theoretically generated temporal profiles of Fig. 2. The spikey character of the profile is due to beating of the longitudinal laser modes. The full width at half maximum of 30 pulses was measured and the mean was found to be 9 ± 1 nsec. We saw no recurrent patterns in the temporal profile of the laser pulses from shot to shot. The temporal shape looked different for each pulse. The model assumption we used of a random phase for each mode is consistent with these observations, although we note that some coherence has been observed in similar dye lasers.[12] The validity of this "random-phase" approximation is addressed further in the discussion section.

The atomic-hydrogen source[13] and interaction region are shown in Fig. 7. Molecular hydrogen gas was dissociated at a pressure of 200 torr by a rf discharge in a Pyrex tube surrounded by liquid nitrogen. A photodiode and an interference filter were used to monitor the amount of Balmer α radiation coming from the discharge. A 2-mm orifice limited the flow of hydrogen atoms into the interaction region. The pressure in the interaction region was 1×10^{-5} torr when atomic hydrogen was flowing. An indium seal separated the liquid-nitrogen reservoir

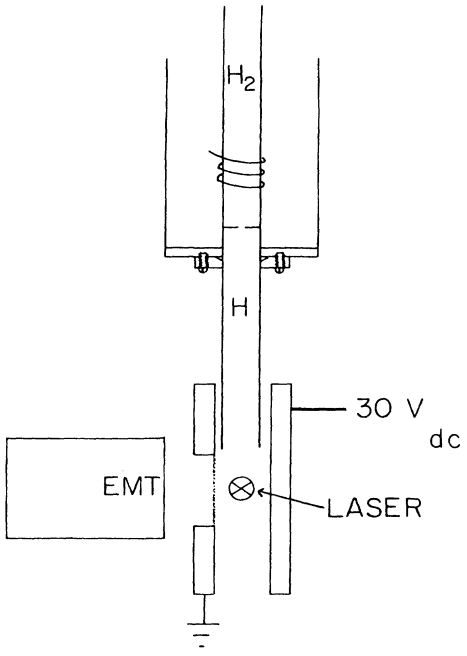

FIG. 7. Schematic view of the atomic-hydrogen beam source. Indicated in the figure are also the interaction region of the hydrogen with the laser light and the electron-multiplier tube (EMT) used for the ion detection.

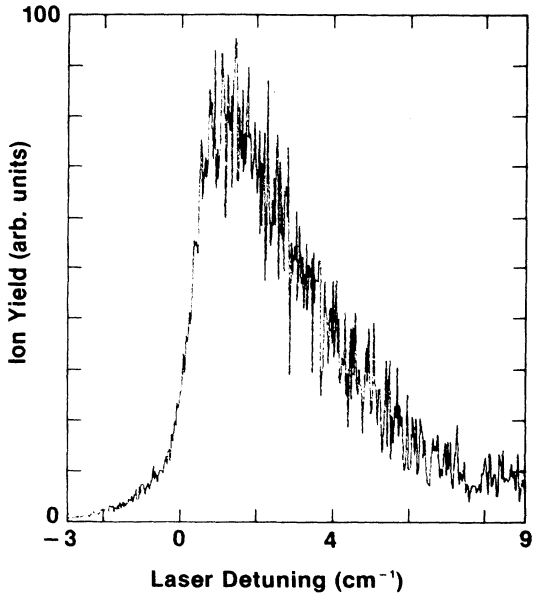

FIG. 8. Hydrogen ionization signal as a function of the single-photon detuning $\omega_L-\omega_0/3$, where ω_L is the laser frequency and $\omega_0/3=27\,419.7\ \mathrm{cm}^{-1}$.

from the vacuum region. 10 W of rf power were transferred from the rf source to the load. The density of atomic hydrogen in the interaction region was measured to be $\sim 10^{11}$ atoms/cm^3 using a platinum recombination detector.[14]

The laser intersected the atomic beam at right angles. H^+ ions created by resonant multiphoton ionization were swept by a pair of field plates through a grid to the detector. The fast linear focused electron multiplier detector was manufactured by EMI, No.D233B. The detector linearity was carefully verified.

The experiment consisted of measuring the resonance-ionization profile, i.e., the ionization yield as a function of laser frequency. The profile was measured over a range of different laser-pulse energies. The ionization signal from 16 laser shots was averaged at a specific laser frequency and stored in a computer channel. The laser was then scanned by computer to the next frequency. 450 computer channels correspond to a 12-cm^{-1} scan at 365 nm. An iodine absorption signal was simultaneously recorded by the computer. A typical profile is shown in Fig. 8. The laser detuning is defined as $\omega-\omega_0/3$, where ω is the laser frequency and $\omega_0/3=27\,419.7\ \mathrm{cm}^{-1}$ is one-third the energy of the $1s$-to-$2p$ transition.

IV. DISCUSSION AND RESULTS

A. Competing ionization mechanisms

It was important to experimentally determine that the observed ionization signal resulted from resonant four-photon ionization rather than some other nonlinear process. To check for photodissociation of dimers $H_2\rightarrow H+H$ and photoionization of dimers $H_2\rightarrow H_2^+ + e$ we tuned to the peak of the resonance-ionization profile. The laser-pulse energy was 7 mJ and the ion signal was approximately 1 V across 50 Ω. When the rf discharge was turned off the signal disappeared. The electron-multiplier bias was then increased by 1000 V. An ionization signal was still not observed.

Nonresonant four-photon ionization was experimentally ruled out as a competing process by the lack of a detected constant background signal on the blue side of threshold. In addition, using a Soleil-Babinet compensator to produce circularly polarized light produced no observable signal. Only nonresonant photoionization is allowed in this case because the dipole selection rule for circularly polarized light does not allow three-photon transitions between the $1s$ and $2p$ states.

Third-harmonic generation in atomic hydrogen was ruled out for our experimental conditions by the null result we obtained in searching for Lyman-α light. By using a Lyman-α detector we were able to determine that less than 3×10^{-3} of the multiphoton ionization signal could be attributed to Lyman-α generation in atomic hydrogen.

B. Line shape, line shift, and linewidth

The resonance-ionization profile shown in Fig. 8 has several notable features. (1) The line shape is asymmetric, with a pronounced blue wing. (2) The peak of the profile is shifted to the blue ($\omega_{\mathrm{peak}}-\omega_0/3>0$). (3) The width of the profile significantly exceeds the laser bandwidth, one-third the $2p$-state fine-structure splitting, and also Doppler width and collisional and radiative widths. (4) The blue side of the profile exhibits significantly more noise than the red.

The shape of the profile can be compared to that predicted from the theoretical model discussed in Sec. II. The experimental and theoretical profiles are shown in Fig. 9. The experimental profile has been smoothed using a simple three-point average. The height of the theoretical profile was normalized to that of the measured profile. Also, we had to assume a laser-pulse energy that was 20% lower than measured, but within experimental error, to get good agreement with the measured width. The line shapes agree quite well.

In this paper we define the width of the resonance-ionization profile as the full width at half maximum. The shift is defined as the frequency of the bisector of the profile at half maximum, minus $\frac{1}{3}$ the $1s$-$2p$ transition frequency, $\omega_0/3$. We measured the width as a function of the laser-pulse energy. Figure 10 shows the variation of the ionization profile with the laser-pulse energy. The profiles are offset for purposes of display and each profile was recorded with a different detector gain to permit the highest signal-to-noise ratio. These profiles have been smoothed using a simple three-point average. The shift and width was measured for each profile. The result is shown in Fig. 11 along with the width and shift predicted by the theoretical model. The shift and width vary linearly with laser intensity, as expected. Although there is a systematic deviation of the data points from the

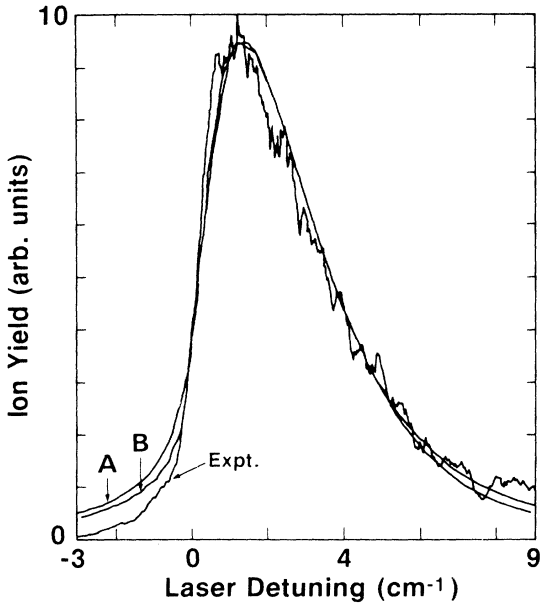

FIG. 9. Experimental and theoretical resonance-enhanced ionization profiles as a function of the single-photon laser detuning $\omega-\omega_0/3$, where $\omega_0/3=27\,419.7\ \mathrm{cm}^{-1}$. The curve labeled A represents the theoretical curve of Zoller [Eq. (21) of Ref. 4] and B represents our model described in the text. The laser-pulse energies of the A (4.3-mJ) and B (5.8-mJ) curves were chosen so that the FWHM's of these curves were the same as the experimental curve (7.1 mJ).

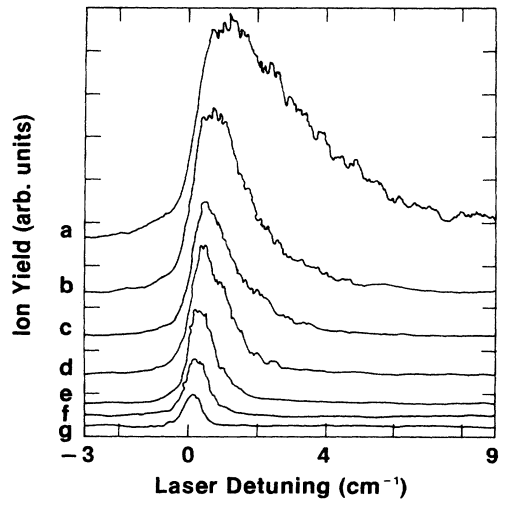

FIG. 10. Variation of the ionization signal profile with the laser-pulse energy. The frequency scale is the same as in Fig. 8. The individual curves are obtained with laser energies in mJ: (a) 7.1, (b) 4.2, (c) 3.4, (d) 2.5, (e) 1.7, (f) 0.8, (g) 0.4. The signals are offset for the purpose of display.

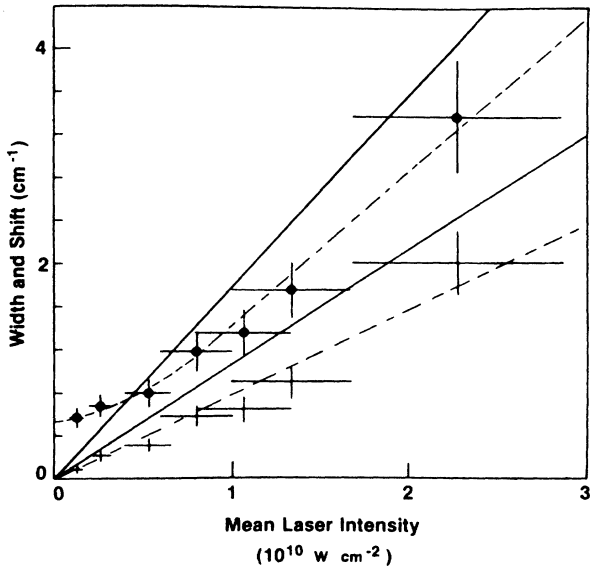

FIG. 11. The width (black dots) and shift of the resonance profiles displayed in Fig. 10 are plotted as a function of the mean laser intensity at the spatial and temporal center of the uv pulse. The solid lines are the theoretical predictions. The width is the upper line and the shift is the lower line. The dashed lines were fitted by hand to the data.

theoretically generated lines, this deviation is within the estimated experimental error.

At low intensity the measured width departs from a straight line and is dominated by the laser linewidth (0.25 cm^{-1}), Doppler (0.17 cm^{-1}/photon), and fine-structure (0.12 cm^{-1}/photon) widths of the $2p$ state. The estimated net width, 0.42 cm^{-1}, is the maximum residual width at zero intensity. This value agrees well with the value extrapolated from the data, $0.5\pm0.1\ \mathrm{cm}^{-1}$.

The shift-to-width ratio is an intensity-independent parameter. This was derived from resonance profiles measured at the highest laser-pulse energies taken from eight independent sets of data. The mean of 0.61 ± 0.04 (one standard deviation) agrees well with the value generated by the theoretical model, 0.56. This value from the observed profile is quite different from the theoretical ratio $\delta/\gamma=1.26$ for a uniform field. This is because the distribution of shifts associated with different values of the radiative fields increases the apparent width of the profile.

C. Laser-intensity dependence of the ion yield at the peak of the resonance profile

The measurement of the laser-intensity dependence of the ionization yield is a further test of resonant multiphoton ionization theory.

As discussed in Sec. II, the intensity dependence of the ion yield at the peak of the resonance-ionization profile is expected to be quadratic. This can be shown to be independent of the spatial or temporal variations in the laser intensity, in the limit when a large number of laser

shots is averaged.[8] An important provision is that the ionization width $\gamma/2\pi \gg B$. At our highest "mean" laser intensity, $\gamma/2\pi = 6.8\ \text{cm}^{-1}$, we note that the theoretical model predicts instantaneous peak laser intensities that are a factor of 4–5 larger than this mean. Most of the ionization takes place in the high-intensity spikes. The laser bandwidth is 0.25 cm^{-1} (FWHM), so the condition $\gamma/2\pi \gg B$ is satisfied. (In the large-laser-bandwidth limit $\gamma/2\pi \ll B$ the intensity dependence is predicted to be cubic.)

Profile peak exponents between 2 and 2.5 for three-photon resonant, four-photon ionization have been measured in an experiment in Cs (see Fig. 10 of Ref. 15 and Fig. 8 of Ref. 16) and have been attributed to laser bandwidth,[15] Doppler effect,[15] fine-structure effects, and to radiation fields which fluctuate during the ionization time of the resonant state.[16]

During the experimental runs the laser-pulse energy was kept constant to within 10% during the scan. The rf power to the hydrogen discharge, the H_2 pressure, and the Balmer-α monitor were all constant during an experimental run. Seven sets of data were taken with laser-pulse energies between 1 and 11 mJ.

In Fig. 12 the peak intensity of the resonance profile is plotted versus the laser-pulse energy on a log-log scale. The data were fitted to a straight line. In this higher-laser-pulse-energy range the measured intensity exponent m of the peak of the ion-yield profile was $m = 2.3 \pm 0.1$. The indicated errors represent one standard deviation.

The intensity dependence in the higher-pulse-energy range, $I^{2.3\pm0.1}$, differs somewhat from the I^2 dependence that our model predicts. Deviations from I^2 behavior are expected to be due to nonadiabatic effects, as discussed in Sec. II. The nonadiabatic theory of Ref. 4 predicts an $I^{2.2}$ dependence for our conditions (at higher pulse energy and after spatial averaging).

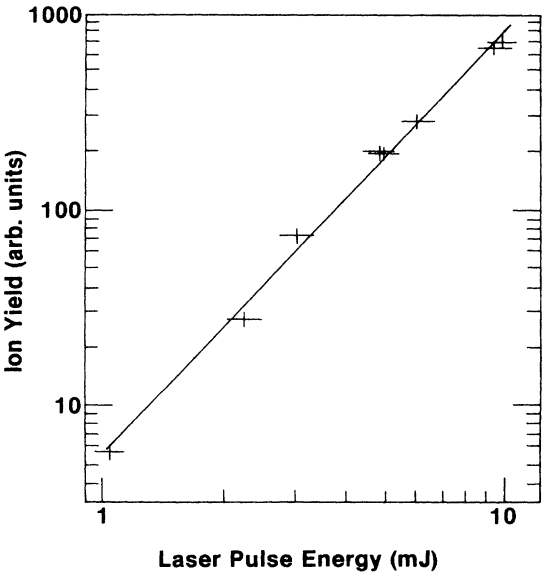

FIG. 12. Peak ion yield vs laser-pulse energy in the high-laser-energy regime ($1 \lesssim E \lesssim 11$ mJ). The solid line represents a least-squares fit to the data with a straight line yielding a slope of $m = 2.3 \pm 0.1$.

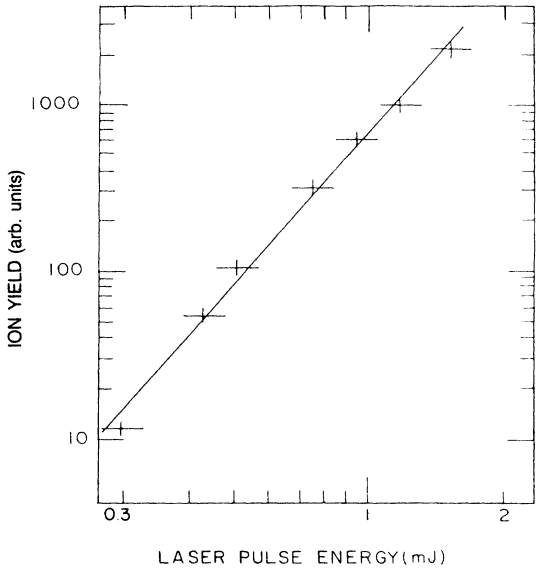

FIG. 13. Peak ion yield vs laser-pulse energy in the low-laser-energy regime ($0.3 \lesssim E \lesssim 1.5$ mJ). A least-squares fit to the data by a straight line (solid line) yields a slope of $m = 3.0 \pm 0.2$.

Three sets of data were taken at low laser-pulse energies between 0.3 and 1.5 mJ. In Fig. 13 a similar plot is displayed for this low-pulse-energy range. In this energy range the measured intensity exponent was measured to be $m = 3.0 \pm 0.2$. In this energy range the fine structure, Doppler, and laser linewidth of the $2p$ state dominate the linewidth of the profile. In this regime the intensity dependence of the ion yield at the peak of the profile is expected to vary cubically with laser intensity. The measured intensity dependence confirms this.

D. Discussion of the photon-statistical properties of the dye laser

Recently Westling and Raymer[12] have undertaken detailed investigations of the relative mode amplitudes and phases of a multimode grazing-incidence dye laser. Their modeling of intensity autocorrelation functions for observed pulses demonstrates that for certain configurations of their laser cavity, the mode-intensity distribution is clearly non-Gaussian, and for other configurations they determine that the mode phases are locked together. Our single-shot spectral measurements indicate a Gaussian distribution of mode intensities for our laser. While we do not have a direct measure of the relative phases of the modes, the random-phase approximation that we have made does give a good approximation to the variety of observed temporal profiles of our pulses, as well as a good fit to the observed ionization line profiles. Finally, we note that the role of the multimode Nd:YAG pump laser

has not been explicitly included in our model for the photon statistics. In general, the mode structure and temporal behavior of the pump laser can influence the corresponding behavior of the dye laser. Also, in our experimental configuration in which we sum mix the output of the dye laser with the fundamental of the pump laser, the resulting photon statistics can be a complex admixture of the two inputs. We assume here, however, that if the phases are largely random, it is sufficient to incorporate these statistical contributions via their effect on the net bandwidth of the pulse used to photoionize the atoms.

V. CONCLUSIONS

We have measured the line shape of the resonant four-photon multiphoton ionization of atomic hydrogen. In particular, we have measured the width, shift, asymmetry, and peak height of the resonance-ionization profile as a function of laser intensity. These measurements agree well with the predictions of our theoretical model of resonant multiphoton ionization. The model explicitly takes into account the spatial and temporal variations of the radiative field of our multimode laser. The agreement between our experimental measurements and the model confirms the values of the parameters Ω, δ, and γ provided to us by Reinhardt.[5]

Except at our lowest laser intensities, the width of the observed resonant-enhanced photoionization profile significantly exceeded the Doppler width, radiative decay rate, and laser bandwidth. This latter condition is particularly important because it is essential to justify the use of Eq. (1) in modeling the effect of the radiative field fluctuations on the profile.

The width and shift of our experimental profile were observed to vary linearly with laser intensity (except for the width at low intensities, due to Doppler and laser-bandwidth contributions). The magnitude of the measured width and shift are about 20% smaller than predicted by the model on the basis of our measured laser-intensity distribution. This discrepancy is just within the limit of what we estimate to be the uncertainty in our laser-intensity measurements, which stem from the determination of the spatial and temporal distribution of the laser pulse, in addition to the total energy measurement. Except at our lowest intensities, the width-to-shift ratio was measured to be independent of laser intensity.

The shape of the observed ionization profile is highly asymmetric, with a long tail towards the blue and a relatively fast dropoff of the red wing. This latter effect appears to be unrelated to the fact that the photoionization occurred near threshold. In fact, the entire profile, including the steep red wing, are in good agreement with models which do not include explicitly any threshold energy effect. The asymmetric shape as a whole reflects the distribution of ac Stark shifts (quadratic in the field) which arises from the distribution of intensities in the laser pulse.

The details of the shape, shift, and width depend on the mode structure of the laser. The width and ionization yield can be on the order of 3–5 times larger for a multimode laser than for a single-mode pulse of the same energy and pulse duration. The shape of the experimental profile agrees well with two different models. Our model, described earlier in the text, numerically simulates the mode structure of the laser in great detail, but assumes that the radiative field fluctuations are slow compared to the photoionization rate of the excited state. The analytic model of Zoller[4] assumes a finite-bandwidth chaotic field characterized by Gaussian statistics, but makes no other assumptions except that depletion of the ground state is small. The shape of Zoller's predicted profile agrees well with both our measured and calculated profiles. This is consistent with the fact that the effect of a multimode laser field should approach that of a chaotic field as the number of laser modes becomes large. (We note, however, that the analytic results of Zoller[4] have not been averaged over the spatial distribution of intensities at the focus of a laser.)

The measured intensity dependence of the peak of the ionization profile agrees with the predictions of our model–quadratic for intensities such that $\gamma \gg B$, and cubic when $\gamma \ll B$.

It would be very desirable to make observations using this same excitation at higher laser intensities to study threshold effects such as those discussed in Ref. 17. Such measurements would have to be done with much shorter laser pulses to avoid depletion of the ground state.

ACKNOWLEDGMENTS

The experimental part of this work was performed in the laboratory of Daniel Kleppner; we are indebted to him for the use of his facilities and his assistance. We also thank William Reinhardt for providing us with essential theoretical data and Jinx Cooper for useful discussions. This work was supported in part by the U. S. Air Force Office of Scientific Research under Contract No. ISSA-87-0005. One of us (F. B.) was supported by a grant from the Deutsche Forschungsgemeinschaft.

APPENDIX

The general density-matrix equations governing multiphoton processes are discussed in Ref. 6. Following the development of Ref. 6 we expand the general density-matrix elements in terms of harmonics of the incident field frequency,

$$\rho_{ab}(t)=\sigma_{ab}(t)+\sum_{n>0}[\sigma_{ab}^{(n)}(t)e^{in\omega t}+\sigma_{ba}^{(n)*}(t)e^{-in\omega t}] . \tag{A1}$$

After adiabatic elimination of all elements other than σ_{11}, the population in the $1s$ state, σ_{22}, the population in the $2s$ state, and $\sigma_{12}^{(3)}$, the remaining equations governing the secular evolution of these elements are

$$\frac{d\sigma_{11}(t)}{dt}=\gamma_s\sigma_{22}(t)+2\,\mathrm{Im}\{\mu_{12}^{(3)*}\sigma_{12}^{(3)}(t)[\varepsilon^*(t)]^3\} , \tag{A2}$$

$$\frac{d\sigma_{22}(t)}{dt}=-[\gamma_i(t)+\gamma_s]\sigma_{22}(t) -2\,\mathrm{Im}\{\mu_{12}^{(3)*}\sigma_{12}^{(3)}(t)[\varepsilon^*(t)]^3\} , \tag{A3}$$

$$\frac{d\sigma_{12}^{(3)}(t)}{dt}=-i\{[3\omega_L-\omega_{12}-\delta(t)]+\tfrac{1}{2}[\gamma_i(t)+\gamma_s]\}\times\sigma_{12}^{(3)}(t)+i[\sigma_{22}(t)-\sigma_{11}(t)]\mu_{12}^{(3)}[\varepsilon(t)]^3\ , \tag{A4}$$

where the notation is the same as that used in the body of the paper and γ_i and γ_s are the ionization and spontaneous emission loss rates from the $2p$ state, respectively. Note that the complex field amplitude $\varepsilon(t)$ is now time dependent. Formal integration of Eq. (A4) yields an expression for $\sigma_{12}^{(3)}(t)$ which can be substituted in Eqs. (A2) and (A3) to give equations for $\sigma_{11}(t)$ and $\sigma_{22}(t)$, the populations in the $1s$ and $2p$ states, respectively. The equation for $\sigma_{22}(t)$ becomes

$$\frac{d\sigma_{22}}{dt}=-[\gamma_i(t)+\gamma_s]\sigma_{22}(t)-2\,\mathrm{Re}\left\{|\mu_{12}^{(3)}|^2\int_0^t\varepsilon^3(t)\varepsilon^{*3}(t')\exp\left[i\left[(3\omega_L-\omega_{12})(t'-t)+\int_{t'}^t\delta(t'')dt''+i\int_{t'}^t\frac{\gamma_i}{2}(t'')dt''\right]\right]\times[\sigma_{22}(t')-\sigma_{11}(t')]dt'\right\}. \tag{A5}$$

In the time regime in which the process can be treated perturbatively, i.e., when depopulation of the ground state is negligible, we can set $\sigma_{22}-\sigma_{11}=-1$. In addition, when the ionization rate of the $2p$ state is rapid compared to the rate of transitions between the $1s$ and $2p$ states the repopulation of the ground state will be negligible. In this case the second term of Eq. (A5) can be regarded both as the instantaneous rate of population of the $2p$ state, and of multiphoton ionization. Thus

$$R(t)=2\ \mathrm{Re}\left\{|\mu_{12}^{(3)}|^2\int_0^t\varepsilon^3(t)^*\varepsilon^3(t')\exp\left[i\left[(3\omega_L-\omega_{12})(t'-t)+\int_{t'}^t\delta(t'')dt''+i\int_{t'}^t\frac{\gamma_i}{2}(t'')dt''\right]\right]dt'\right\}. \tag{A6}$$

If the complex field amplitude $\varepsilon(t)=|\varepsilon(t)|e^{i\theta(t)}$ is known explicitly for all times then Eq. (A6) can be integrated over the history of the laser field to give the instantaneous rate of ionization $R(t)$. This process is simplified greatly in the limit where the field fluctuations occur on a time scale which is slow compared to the time characterizing ionization of the $2p$ state, i.e., $\gamma/2\pi\gg B$. In this case the exponential factor $\exp[-\int_{t'}^t\gamma_i(t'')dt'']$ in the integrand of Eq. (A6) ensures that the integrand will be vanishingly small for values of t' which are very different from the upper limit of integration t. Thus we can expand the integrand to first order in t' about t which yields the following expression for $R(t)$:

$$R(t)\approx 2\,\mathrm{Re}|\mu_{12}^{(3)}|^2|\varepsilon(t)|^6\int_0^t d\tau\exp\left\{-i\left[(3\omega_L-\omega_{12})-3\dot\theta(t)-\delta(t)-i\left[\frac{\gamma_i(t)}{2}+3\left|\frac{\dot\varepsilon(t)}{\varepsilon(t)}\right|\right]\right]\tau\right\}. \tag{A7}$$

Integration of (A7) gives

$$R(t)=2|\mu_{12}^{(3)}[\varepsilon(t)]^3|^2\frac{\frac{\gamma_i(t)}{2}+3\left|\frac{\dot\varepsilon(t)}{\varepsilon(t)}\right|}{[3\omega_L-\omega_{12}-3\dot\theta(t)-\delta(t)]^2+\left[\frac{\gamma_i(t)}{2}+3\left|\frac{\dot\varepsilon(t)}{\varepsilon(t)}\right|\right]^2}. \tag{A8}$$

Since $\dot\theta$ and $|\dot\varepsilon/\varepsilon|$ are both of order B, is the bandwidth of the laser, and since we have already assumed that $\gamma,\delta\gg B$, the instantaneous rate of ionization can be approximated as

$$R(t)=|\mu_{12}^{(3)}[\varepsilon(t)]^3|^2\frac{\gamma_i(t)}{[3\omega_L-\omega_{12}-\delta(t)]^2+\left[\frac{\gamma_i(t)}{2}\right]^2}, \tag{A9}$$

which is identical to Eq. (1).

Alternatively, if the statistics of the field are known, an effective ionization rate can be calculated by averaging Eq. (A6) over the field fluctuations characteristic of the relevant correlation functions of the field. This has been accomplished for fields with a constant mean intensity and a Lorentzian frequency spectrum by Zoller in Ref. 4.

*Present address: Lawrence Livermore National Laboratory, Livermore, CA 94550.
†Present address: Department of Physics, McGill University, Montreal, Québec, Canada H3A 2B2.
‡Present address: Department of Physics, Bucknell University, Lewisburg, PA 17837.

[1]J. H. Tjossem and T. A. Cool, Chem, Phys. Lett. **100**, 479 (1983); M. Alden, A. L. Schawlow, S. Svanberg, W. Wendt, and P. -L. Zhang, Opt. Lett. **9**, 211 (1984).
[2]D. E. Kelleher, M. Ligare, and L. R. Brewer, Phys. Rev. A **31**, 2747 (1985).
[3]C. R. Holt, M. G. Raymer, and W. P. Reinhardt, Phys. Rev. A **27**, 2971 (1983).
[4]P. Zoller, J. Phys. B **15**, 2911 (1982).
[5]W. P. Reinhardt (private communication).
[6]A. T. Georges, P. Lambropoulos, and J. H. Marburger, Phys. Rev. A **15**, 300 (1977).
[7]D. S. King and R. R. Cavanagh, Opt. Lett. **8**, 18 (1983).
[8]M. Ligare (unpublished).
[9]H. Zacharias, H. Rottke, J. Danon, and K. H. Welge, Opt. Commun. **37**, 15 (1981).
[10]R. Wallenstein and H. Zacharias, Opt. Commun. **32**, 429 (1980).
[11]M. G. Littman and H. J. Metcalf, Appl. Opt. **17**, 2224 (1978).
[12]L. A. Westling and M. G. Raymer, J. Opt. Soc. Am. B **3**, 911 (1986); L. A. Westling, Ph. D. thesis, University of Rochester, 1986 (unpublished); L. A. Westling, M. G. Raymer, and J. J. Snyder, J. Opt. Soc. B **1**, 150 (1984).
[13]L. R. Brewer, Ph. D. thesis, Massachusetts Institute of Technology, 1984 (unpublished).
[14]D. Brenner, Rev. Sci. Instrum. **40**, 4307 (1981).
[15]L. A. Lompre, G. Mainfray, C. Manus, and J. P. Marinier, J. Phys. B **14**, 4307 (1981).
[16]G. Petite, J. Morellec, and D. Normand, J. Phys. **40**, 115 (1979).
[17]Shih-I Chu and J. Cooper, Phys. Rev. A **32**, 2769 (1985).